Morphological transformation of the process zone at the tip of a propagating crack. II. Geometrical parameters of the process zone

Alexei Boulbitch[1,*] and Alexander L. Korzhenevskii[2]
[1]*Zum Waldeskühl 12, 54296 Igel, Germany*
[2]*Institute for Problems of Mechanical Engineering, RAS, Bol'shoi prosp. V. O. 61, 199178 St. Petersburg, Russia*

(Received 8 December 2018; accepted 11 February 2020; published 11 March 2020)

The morphological transformation of the process zone at the tip of a propagating crack occurs with the increase of the crack velocity. The zone configuration changes its shape from concave to convex, dropletlike form. The latter exhibits a metastable wake. We prove that the transformation takes place as soon as the crack velocity exceeds Gordon's speed V_G. The latter is the velocity of motion of the interface between the stable and overheated metastable phases. We further analyze the dependence of geometrical parameters of the zone and wake on the crack tip velocity. We show that at a constant velocity, the size of the process zone grows with the approach to the binodal. However, it decreases by over three orders of magnitude as the crack's velocity increases. In contrast, the interval length where the zone or the wake comes in direct contact with the crack surface increases at $0 \leqslant V < V_G$, achieves its maximum at $V = V_G$, and then decreases with the further velocity increase. The zone vanishes as soon as the crack's velocity exceeds a critical speed V_{cr}.

DOI: 10.1103/PhysRevE.101.033004

I. INTRODUCTION

This paper is the second part of our communication, started with [1]. We addressed a crack tip process zone, a local phase transition of the first order taking place at the tip of a propagating crack due to the stress concentration in its vicinity. One observed this phenomenon in numerous solids exhibiting different chemical compositions and crystal structures. A detailed review of various experiments detecting the process zone we have communicated in the introduction to the previous paper [1].

We studied the process zone within the field-theoretical approach numerically [1]. In this approach the process zone is described by the stress field as well as by the field of the *order parameter,* as prescribed by the Landau theory of phase transitions [2,3]. We have proved [1] that one can exhaustively describe the problem by the dynamic equation

$$2^{1/3}\frac{\partial u}{\partial \tau} = \Delta u - [a - \widetilde{U}(r,\theta,\tau)]u + bu^3 - u^5 = 0 \qquad (1)$$

with the boundary condition $u|_{\partial\Omega} = 0$. Here, τ is dimensionless time, x and y are dimensionless spatial variables, and $u = u(x, y, \tau)$ is the dimensionless order parameter. Further, Ω is the domain, $\partial\Omega$ is its boundary, $\Delta u = \partial^2 u/\partial x^2 + \partial^2 u/\partial y^2$ is the dimensionless two-dimensional (2D) Laplacian, $a > 0$ and $b > 0$ are the dimensionless control parameters. Finally, $\widetilde{U}(r, \theta, \tau)$ is the contribution of the crack tip stress. In terms of the cylindrical coordinates r and θ counted off from the crack tip: $r = [(x - v\tau)^2 + y^2]^{1/2}$ and $\theta = \arctan[y/(x - vt)]$ it takes the following form:

$$\widetilde{U}(r,\theta) = \frac{\sqrt{2}\cos(\theta/2)}{r^{1/2}}. \qquad (2)$$

We study the crack propagating along the line $y = 0$ from left to right with dimensionless velocity v. In the comoving system of coordinates $(x - v\tau, y)$, the automodel equation on $u = u(x - v\tau, y)$ takes the form

$$\Delta u + 2^{1/3} v\frac{\partial u}{\partial x} - [a - \widetilde{U}(r,\theta)]u + bu^3 - u^5 = 0. \qquad (3)$$

Here, $u(x - v\tau, y)$ describes the running zone. Equations (1), (3), and (2) are obtained by elimination of elastic variables form the full system of equations followed by rescaling of the resulting equation of motion. Their detailed derivation along with the discussion can be found in the first part of our paper [1].

A numerical study of Eq. (3) has been performed by the finite element method in the phase diagram region, where the daughter phase is metastable while the mother phase is stable. We fixed the value of the parameter $b = 1$ and simulated Eq. (3) at four a values: 0.2, 0.22, 0.23, and 0.24. All of these values lie above the binodal, $a_b = 3b^2/16$, but below the upper spinodal, $a_{up} = b^2/4$(see Fig. 1 of the previous paper [1]).

At all the values of the parameters, we observed the same kind of the zone behavior. At low velocities ($0 \leqslant v < v_G$) the zone had the concave shape resembling a distorted cardioid [as is schematically shown in Fig. 1(a)]. At a particular velocity value $v = v_G$, the invagination in the zone configuration vanished [the form shown in Fig. 1(b)] and at $v_G < v < v_{cr}$ the zone had the shape of a droplet with the pointed end and exhibited a triangular *wake*, the zone remnants behind the zone [indicated by (iii) in Fig. 1(c)]. The wake propagates together with the crack and the zone as a whole. Finally, at $v = v_{cr}$ the zone vanished, and at $v > v_{cr}$ no zone took place at the crack tip.

In [1] we, thus, reported a discovery of a morphological transformation of the zone shape taking place at the velocity $v = v_G$, and vanishing of the zone at $v = v_{cr}$. In this paper,

*Corresponding author: boulbitch@gmx.de

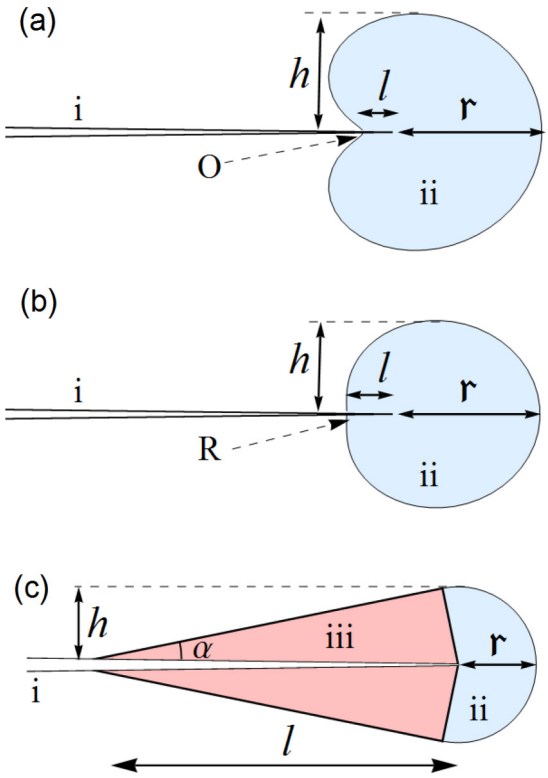

FIG. 1. Schematic view of the process zone and wake at the tip of a propagating crack. (i) Shows the crack position schematically, (ii) indicates the zone, (iii) points out the metastable wake. (a) Shows the zone configuration in the case of small propagation velocity v. (b) The one at $v = v_G$. (c) The zone-wake configuration at a high propagation velocity $v_G < v < v_{cr}$. The parameter l indicates the distance between the crack tip and the deepest invagination point in the case (a), the distance from the tip to the rear zone end (b), and the wake length (c).

we present values of the geometrical parameters of the zone extracted during the numerical experiments described in Ref. [1]. In particular, we show that the sizes of the zone exhibit the highest values at $v = 0$, monotonously decrease with increasing v, and discontinuously turn into zero at $v \geqslant v_{cr}$. In contrast, the contact length l of the concave zone increases with the velocity at $0 \leqslant v \leqslant v_G$ and achieves its maximum at $v = v_G$. At $v_G < v < v_{cr}$ the contact length of the wake dramatically decreases, the rear part of the wake becoming sharper. We estimate the absolute values of the zone parameters and the velocities v_G and v_{cr}. We further discuss available experimental data in the light of our findings.

This paper is organized as follows. In Sec. II, we deliver our numerical data. In Sec. III, we apply our relations to available experiments and discuss our findings.

II. GEOMETRIC PARAMETERS FROM NUMERICAL EXPERIMENTS AND THEIR COMPARISON WITH ANALYTICAL PREDICTIONS

Our simulations enable us to numerically find all important geometric parameters of the zone playing any role in formation of the transformation toughness. Following, we communicate the behavior of the geometric parameters at various crack velocities.

The process zone can be characterized by the distance from the crack tip to the leading point of the zone $\mathfrak{r}$, referred to as its *width*, and the distance h from the crack plane, $y = 0$ to the highest zone, its *height* [Figs. 1(a)–1(c)]. At small velocities, the concave zone can be also characterized by the distance l between the crack tip and the bottom of the zone invagination [indicated by the point O in Fig. 1(a)]. In turn, the wake parameters are the semivertex angle α and the distance l between the tip and the trailing point of the wake [Fig. 1(c)]. All these parameters are indicated in Fig. 1.

Let us recall that the parameters v, $\mathfrak{r}$, h, and l are dimensionless. Below their sizes are given in dimensionless units. We pass to the "physical" dimensions in the Discussion section.

A. Velocity of the shape transformation

The overheated metastable phase "melts down" by way of a motion of the interphase boundary, the order parameter obeying the time-dependent Ginzburg-Landau equation (3). If this phase is stress free, then the potential $\widetilde{U}(r, \theta)$ in (3) should be set strictly to zero.

One can regard Eq. (3) as a nonlinear eigenproblem. The role of the eigenvalue here plays the velocity $v = v_G$. Determination of its value is a part of the solution. An exact eigenvalue of the velocity v_G of the plane metastable phase boundary has been found by Gordon [4,5]. In the case of Eq. (3) the expression for the Gordon velocity has the following form:

$$v_G = \pm \frac{1}{2^{5/6}3^{1/2}} \frac{8a - b^2 - b\sqrt{b^2 - 4a}}{|b^2 - 2a + b\sqrt{b^2 - 4a}|^{1/2}}. \tag{4}$$

Equation (4) describes the velocity of the plane mother-daughter phase interface under the stress-free conditions. The sign "+" corresponds to an overheated metastable daughter phase. The interface velocity, in this case, is directed into the interior of the domain occupied by the daughter phase. In contrast, the sign "−" corresponds to the overcooled mother phase, the interface velocity pointing outward.

If the phase interface has a curvature $1/\rho$, its velocity $v_G^{(c)}$ is expressed as [6]

$$v_G^{(c)} = v_G - \frac{1}{\rho\sqrt[3]{2}}. \tag{5}$$

Here, the superscript "(c)" indicates that the velocity applies to the phase interface with the curvature. The second term of (5) accounts for the effect of the interface surface tension [6].

Behind the propagating process zone, where θ is close to $\pm\pi$, the contribution of the potential (2) is close to zero, implying that the potential does not stabilize the daughter phase in this domain. For this reason, in the region IV of the phase diagram (shown in Fig. 1 of [1]), the daughter phase left behind the zone turns out to be in the overheated metastable state. One concludes that it "melts down" with Gordon's velocity of the free phase interface v_G.

Three cases can take place here: (i) $v < v_G$, (ii) $v = v_G$, and (iii) $v > v_G$. If the crack velocity v is smaller than v_G, the stress-free part of the daughter-mother phase interface directly

behind the crack tip can catch up with the zone motion. Let us introduce a time $\tau_t \sim h/(v_G - v)$, necessary for the most remote part of the boundary at the distance $\sim h$ from the crack tip to melt down to its surface. Let us consider an initially motionless crack which forms a zone with the height h. Upon the onset of the motion with the velocity $0 < v < v_G$, the zone starts moving together with the tip. The zone remnants, the daughter phase, stay behind the tip and start to melt down. One concludes, therefore, that at $\tau > \tau_t$ the daughter phase behind the tip completely vanishes. No wake can exist in this case. It is schematically shown in Fig. 1(a).

Let us note that the rear zone interface in this region can only propagate with the same speed v as that of the crack tip. However, since $v_G > v$, this can only take place, provided the velocity of the interface is smaller than v_G. The latter can only take place due to a surface curvature according to Eq. (5). It is for this reason that the zone forms the concave configuration [Fig. 1(b)] which slows the velocity of the interface down to the crack tip velocity: $v_G^{(c)}(\rho) = v$. At the trailing point of the zone $\theta = \pm\pi$ this condition yields the curvature radius

$$\rho = \frac{1}{2^{1/3}(v_G - v)}. \tag{6}$$

As soon as $v \to v_G$, the curvature radius diverges. This corresponds to a plain portion of the rear edge of the boundary, normal to the crack surface, as it is indicated by R in Fig. 1(b).

In contrast, if $v > v_G$, the rear part of the daughter-mother phase boundary cannot overtake the zone. Thus, a wake consisting of the metastable daughter phase traveling behind the crack tip zone emerges [Fig. 1(c)]. Assuming that the wake takes the triangular shape, that its pointed end propagates with the velocity v, while the almost plane rear boundary part; with Gordon's speed v_G, one finds that the angle α obeys the simple relation

$$\sin(\alpha) = \frac{v_G}{v}. \tag{7}$$

One concludes that the transformation of the zone shape takes place as soon as the crack speed achieves Gordon's velocity $v = v_G$. In [1], we obtained the velocity v_G corresponding to the zone shape transformation from the direct observation of the order parameter distribution (cf. Fig. 5 from [1]). Namely, we observed that at a certain velocity v the zone invagination vanishes. At this velocity, the rear portion of the zone boundary becomes perpendicular to the crack surface [as indicated by the point R in Fig. 1(b)]. This value of the velocity we assumed to be v_G. Dots in Fig. 2 show Gordon's velocities at different a values obtained in this way. The solid line in Fig. 2 shows the run of Gordon's velocity versus a at the fixed value $b = 1$ according to Eq. (4). The close agreement between the numerical and analytical results supports our arguments.

B. Zone width $\mathfrak{r}$

Figure 3 displays the dependence of the zone width $\mathfrak{r}$ on the crack tip velocity v in the semilogarithmic scale. The dots show the results of the simulations. One concludes that at $v = 0$ the zone width $\mathfrak{r}$ is of the order of $\sim 10^3$ of dimensionless units while decreasing to $\mathfrak{r} \sim 1$ at v close to v_{cr}.

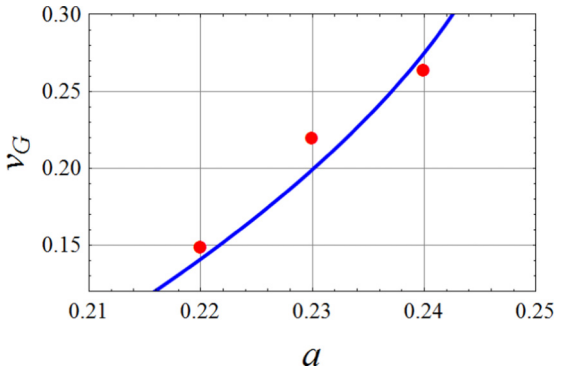

FIG. 2. The solid line shows the dependence of Gordon's velocity v_G on the control parameter a at $b = 1$ according to Eq. (4). The dots indicate the values of the velocities corresponding to the zone shape transformation obtained from simulations.

C. Zone height

Figure 4 shows the dependence of the zone height h on the crack tip velocity on the semilogarithmic scale. The zone height appears to be somewhat smaller than its width (shown in Fig. 3). Qualitatively, however, it exhibits the same behavior: at $v = 0$ one finds $h \sim 10^3$ of the dimensionless units, while drops down to h between 5 and 10 at $v \to v_{cr}$.

Besides, $\log(h) = \log[h(v)]$ exhibits an almost linear dependence on the velocity which is qualitatively analogous to the behavior we observe in the graphic $\log(\mathfrak{r}) = \log[\mathfrak{r}(v)]$ (Fig. 3). The latter stimulates one to look for the dependence of the zone height h on the zone width $\mathfrak{r}$. In the double-logarithmic scale, this dependence is shown in Fig. 5.

This dependence can be accurately approximated by the function

$$h \approx 6.56 \times \mathfrak{r}^{0.73} \tag{8}$$

valid at any a value (the solid line in Fig. 5).

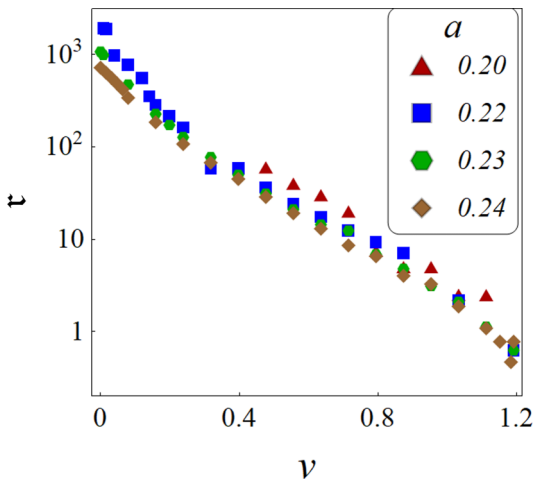

FIG. 3. The semilogarithmic plot of the dependence of the zone width $\mathfrak{r}$ upon the crack velocity v. The dots present the simulation results.

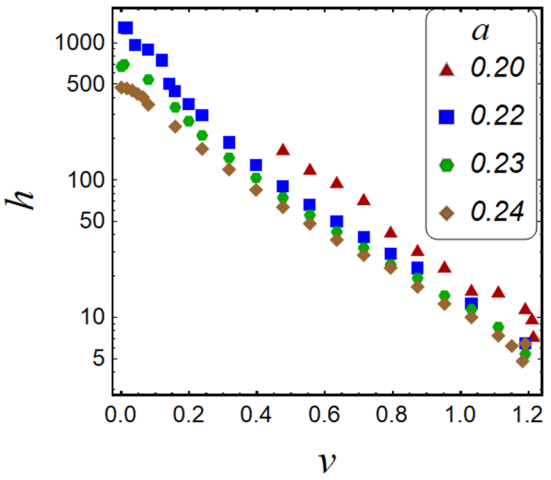

FIG. 4. The semilogarithmic plot of the zone height versus the crack tip velocity according to simulations.

D. Contact length

The *contact length* is the dimension of an interval where the zone (or the wake) directly borders on the crack surface. Let us now turn to study the contact length.

1. Invagination dimension

Under small crack velocities, the process zone exhibits a concave shape characterized by the distance l between the crack tip ($x = y = 0$) and the invagination bottom [the point O in Fig. 1(a)]. The knowledge of this distance plays an essential role because it is on this part of the crack surface that the spontaneous stress exerts the compressive load. Therefore, this part of the crack surface contributes to the transformation toughening. Figure 6(a) shows the dependence of l on the crack tip velocity v in this regime.

Let us stress that at $v = 0$ we observed a finite contact length [Fig. 6(b)] which varies between about 150 at $a = 0.2$ close to the binodal down to about 18 at $a = 0.24$ close to the spinodal.

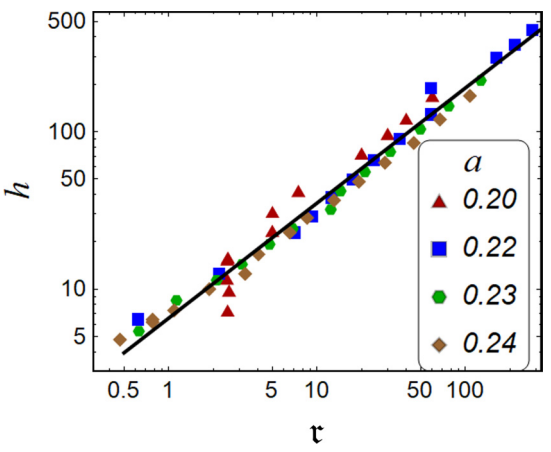

FIG. 5. Dependence of the zone height h on on the width τ. Dots show the results extracted from the simulations. The solid line displays the regression (8).

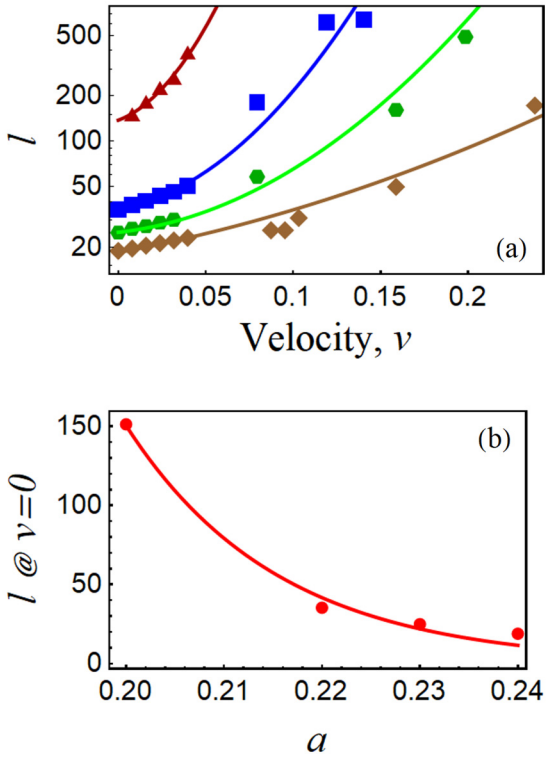

FIG. 6. (a) Dependence of the contact length l on the crack tip velocity v. Triangles $a = 0.2$, squares $a = 0.22$, diamonds $a = 0.23$, and rhombus $a = 0.24$. (b) The contact length of the zone at the motionless crack tip ($v = 0$) depending on the control parameter a. The dots show the results taken from the simulation while the solid lines guide the eye.

2. Wake length

In the velocity interval $v_G < v \leqslant v_{cr}$ the wake forms, and the contact length simultaneously represents the wake length. Figure 7 shows $l = l(v)$ dependence in this regime. Here, one only observes a monotonous decreasing the contact length over two to three orders of magnitude.

E. Semivertex angle of the wake pointed end

At $v_G < v < v_{cr}$ the zone is followed by the wake. The latter has the rear part in the form of a triangle with the semivertex angle α. Figure 8 displays the behavior of α at various crack velocities: the dots in Fig. 8 show the dependence of the semivertex angle α on the crack tip velocity extracted from the simulations, while the solid lines display its behavior according to Eq. (7), which exhibit a good agreement with each other. One observes that the angle becomes more acute as the crack's tip velocity increases. At velocities close to v_{cr} and at $a = 0.2$, close to the binodal a_b, it achieves a value of about 2°, which indicates a stretched out wake with a sharp triangular shape.

F. Critical velocity

In Ref. [1] we reported the observation that as soon as the crack velocity achieves a particular value v_{cr}, close to unity, the process zone disappears. Let us now analyze this phenomenon quantitatively.

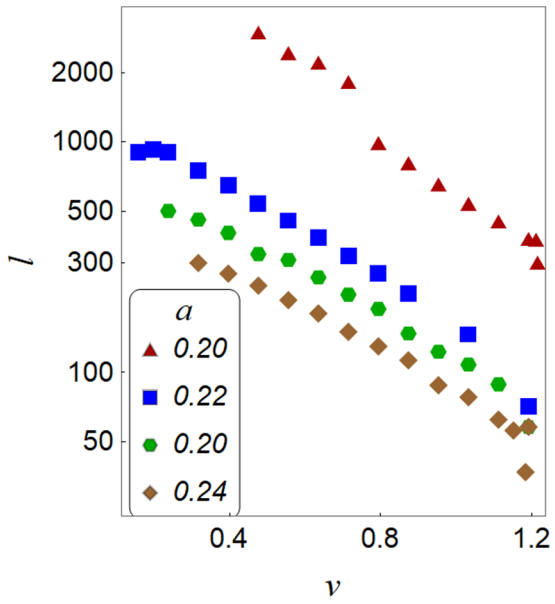

FIG. 7. Dependence of the wake length $l = l(v)$ on the crack tip velocity at various $a = 0.2$, 0.22, 0.23, and 0.24 obtained from our simulations.

It is convenient to analyze the vanishing of the zone by studying its Hilbert norm $I = [\int_\Omega u^2(x, y)dx\,dy]^{1/2}$. Figure 9(a) shows $I = I(v)$, while in Fig. 9(b) we display the blown up vicinity of the critical point. One can see that $I = I(v)$ rapidly decreases with increasing v and has a discontinuity at $v = v_{\rm cr}$. With an increase in the parameter a, the critical velocity decreases Fig. 9(c).

The physical reason for the zone vanishing is as follows. Let us consider a point A in front of the process zone in the direction of its motion. As long as the crack tip is far away from this point, the order parameter here is zero, indicating that the material in the point A is in the mother phase. The order parameter in this point starts responding to the crack approach as soon as the leading edge of the zone comes to the point A over the distance closer than the phase interface

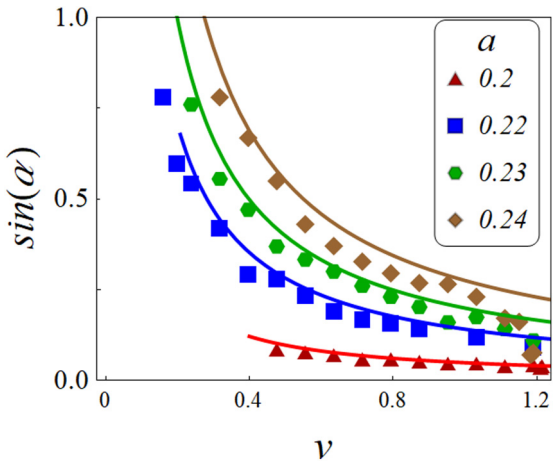

FIG. 8. Dependence of the semivertex angle α at the pointed end of the wake on the crack velocity. Dots show the simulation results, while the solid lines demonstrate the prediction of Eq. (7).

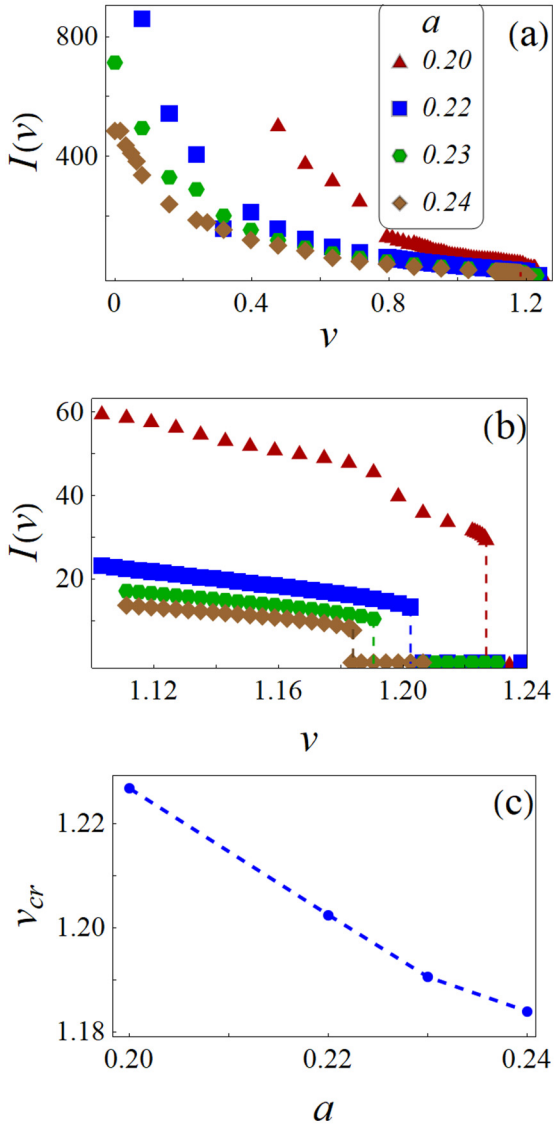

FIG. 9. (a) The behavior of the Hilbert norm I of the solution, depending on the crack tip velocity v. (b) The same behavior in the vicinity of the critical velocity, where the nontrivial solution vanishes. (c) The dependence of the critical velocity on the control parameter a. The dashed line is drawn to guide the eye.

thickness d. By simulations we established $d \sim 1$ dimensionless unit [1]. As soon as the tip is $\sim d$ from the point A, the order parameter reacts by its growth. The growth, however, takes place according to the intrinsic dynamics of the order parameter. The latter has a critical time τ_*. For Eq. (1) it is defined as $\tau_* = 2^{1/3}/a_*$, where a_* is the point at which Eq. (1) exhibits the bifurcation, as we have shown in [7]. Applying the expressions obtained in [7] to the dimensionless equation (1), one finds $a_* = 2^{-2/3}$ and the dimensionless critical time takes the value $\tau_* = 2^{-1/3}$.

While the velocity is small, the order parameter has enough time to emerge as the crack comes closer. However, as soon as the speed exceeds its critical value,

$$v_{\rm cr} \sim \frac{d}{\tau_*}, \tag{9}$$

the time during which the zone approaches the point A becomes insufficient for the order parameter to grow and, hence, the zone cannot appear. In terms of the dimensionless variables, this takes place at $v_{cr} \approx 1.2$.

III. DISCUSSION

A. Passing to dimensional variables

To return to the dimensional variables, time t, spatial coordinates X and Y, order parameter η, and velocity V, one inverts back the rescaling relations introduced in Ref. [1]. For the convenience of the readers, we list the inverted relations following:

$$t = t_0\tau; \quad \begin{pmatrix} X \\ Y \end{pmatrix} = \lambda_0 \begin{pmatrix} x \\ y \end{pmatrix}; \quad \eta = \eta_0 u; \quad V = V_* v. \tag{10}$$

In these expressions t_0 is the characteristic time, λ_0 is the fundamental spatial scale, η_0 is the characteristic order parameter, and V_* is the characteristic velocity of the problem:

$$t_0 = \frac{\kappa g^{1/3}}{2^{1/3}B^{4/3}}; \quad \lambda_0 = 2^{1/3}\left(\frac{g}{B}\right)^{2/3};$$
$$\eta_0 = \frac{B^{1/3}}{2^{1/6}\gamma^{1/4}g^{1/12}}; \quad V_* = \frac{(2g)^{1/3}B^{2/3}}{\kappa}. \tag{11}$$

Here, the factor $B > 0$ controls the interaction between the stress and the order parameter fields. It includes the stress intensity factor K_I in combination with some other material parameters:

$$B = \frac{|A|(1+\sigma)(1-2\sigma)K_I}{E(2\pi)^{1/2}}. \tag{12}$$

Let us stress that while the variables τ, x, y, η, and v are dimensionless, the "physical" parameters τ_0, η_0, and V_*, as well as t, X, Y, η, and V, are dimensional.

In these relations $g > 0$, $\alpha > 0$, $\beta < 0$, $\gamma > 0$, and $A < 0$ are the parameters of the Landau potential, κ is the kinetic factor of the order parameter, E is Young's modulus, and σ is the Poisson ratio. A detailed discussion of these parameters one finds in Ref. [1].

B. Dimensions of the zone and the wake

1. Dependence of the zone and wake dimensions on the velocity and position on the phase diagram

One can characterize the zone and the wake by their dimensions, such as the zone width $\mathfrak{r}$ and height h. We observed that these dimensions dramatically decrease with the crack velocity. In our simulations, these sizes decreased two to three orders of magnitude (as one can see from Fig. 5). Let us note that due to the relations (8) one can regard h as dependent on the zone width $\mathfrak{r}$; they increase or decrease together. In turn, the zone width value strongly depends on the position of the solid on the phase diagram. It has a finite value on the upper spinodal and dramatically increases with approaching the binodal. In the close vicinity of the binodal, the wake length and the zone size can take macroscopic values. Below the binodal, the whole solid passes into the daughter phase.

2. Physical dimensions of the zone

It is essential to get an idea of the physical dimensions of the process zone. One expresses them in terms of the internal spatial scale λ_0 of the problem [1]:

$$\lambda_0 = (4\pi)^{1/3}\left[\frac{gE}{(1+\sigma)(1-2\sigma)AK_I}\right]^{2/3}. \tag{13}$$

This scale may vary considerably for different solids depending on the values of material constants, and decreases with the stress intensity factor: $\lambda_0 \sim K_I^{-2/3}$.

Let us estimate the value λ_0 for $BaTiO_3$ and $PbTiO_3$. For $BaTiO_3$, $g \sim 10^{-14}$ cm^2 and $A \sim 1$ [8], $E \sim 10^{12}$ erg / cm^3, and $K_{IC} \sim 10^7$ erg / cm$^{5/2}$ [9,10]. In the case of $PbTiO_3$, $g \sim 10^{-14}$ cm^2 and $A \sim 1$ [8], $E \sim 10^{12}$ erg / cm^3 and $K_{IC} \sim 10^8$ erg / cm$^{5/2}$ [9,10]. Assuming $K_I \sim K_{IC}$ in both cases of $BaTiO_3$ and $PbTiO_3$ one finds the same estimate of the fundamental dimension: $\lambda_0 \sim 10$ nm.

In our simulations, the dimensionless width $\mathfrak{r}$ of the zone and its height h at small crack velocities achieved the values $\sim 10^3$ dimensionless units. The latter yields the physical width $\mathfrak{R} = \mathfrak{r} \times \lambda_0$ and the height $H = h \times \lambda_0$, of the zone of ~ 10 μm. This estimate agrees with the size of the zone observed in $BaTiO_3$ [11].

Let us note that these sizes critically depend on the closeness of the point of simulation to the binodal. By approaching the binodal, one can increase these sizes unlimitedly. In the vicinity of the critical velocity, the sizes $\mathfrak{R}$ and H in $BaTiO_3$ and $PbTiO_3$ go down to about 50 to 100 nm.

Let us note that the parameters of the expression (13) scarcely vary for different inorganic solids. Indeed, the estimate $E \sim 10^{12}$ erg / cm^3 and $K_{IC} \sim 10^7$ erg / cm$^{5/2}$ are rather typical and in different materials typically vary within one order of magnitude. In different solids, the striction constant A, and the inhomogeneity constant g, however, can vary several orders of magnitude. In such cases, the estimates for λ_0 can also vary considerably.

C. Characteristic velocities

1. Expressions for characteristic velocities

Using (11) and (12) one finds the estimate for the characteristic velocity V_*:

$$V_* \sim \frac{1}{\kappa}\left(\frac{gA^2K_I^2}{E^2}\right)^{1/3}. \tag{14}$$

Passing back from $v_{cr} \approx 1.2$ to the dimensional critical velocity $V_{cr} = v_{cr}V_*$ one finds

$$V_{cr} \sim V_*. \tag{15}$$

2. Estimates of characteristic velocities for some ferroelectrics

Let us estimate $v_G = V_G/V_*$. Direct substitution yields

$$v_G \sim \frac{g^{1/6}E^{2/3}}{(AK_I)^{2/3}} \times \frac{|\beta|}{\sqrt{\gamma}}. \tag{16}$$

In the cases of the ferroelectrics $BaTiO_3$, and $PbTiO_3$, all the parameters of (16) have been measured. One can estimate the values of Gordon's velocity v_G for these materials without assumptions. For $BaTiO_3$, $|\beta| \sim 10^{-13}$ cm^3 / erg and

$\gamma \sim 10^{-23}$ cm^6 / erg^2 [12]. In the case of $PbTiO_3$, $|\beta| \sim 10^{-13}$ cm^3 / erg and $\gamma \sim 10^{-24}$ cm^6 / erg^2 [12]. The values of E, g, A, and K_{IC} we already listed in the previous section. With their use in both materials one finds $v_G \sim 10^{-1}$, hence, $V_G \ll V_*$. Thus, $V_G < V_*$ and, therefore, depending on the crack velocity it can exhibit a concave zone and also a convex zone with triangular wakes.

In particular, one regards $PbTiO_3$ as an intermediate between the order-disorder and displacement type of the transition with $\kappa \approx 0.6 \times 10^{-8}$ s [13]. Making use of the values of the parameters given above for $PbTiO_3$ one finds $V_* \sim 10$ cm / s, $V_G \sim 1$ cm / s. This is in line with the Gordon velocities measured in $PbTiO_3$ at the hysteresis edge [14,15]. To the best of our knowledge, the kinetic factor of $BaTiO_3$ is unknown. Assuming it to be the same as in $PbTiO_3$, one finds $V_* \sim 1$ cm / s and $V_G \sim 10^{-1}$ cm / s.

D. Smooth versus the cusp-shaped zone invagination at the tip of the motionless crack

Let us note that previously, theoretical papers predicted the phase boundary in the form of a perfect cardioid. The latter exhibits a cusp at the crack tip. The origin of such a prediction was a criterion of the phase interface. One used criteria like the ones employed in mechanics to determine the onset of the plastic flow. McMeeking and Evans [16] as well as Budiansky *et al.* [17], for example, assumed the phase boundary to dwell at the place where the stress spur was equal to a specific material constant. Alternatively, one equated the material constant to an invariant combination of the stress tensor components [18]. For a dilatational phase transformation, these criteria always reduce to the stress spur equal to a specific constant. Such a condition inevitably yields the phase interface in the form of a cardioid.

Let us stress that the approaches based on plasticitylike criteria disregard the surface tension of the phase boundary. However, experimental observations, as well as simulations, reported the phase boundary energy for various materials in the range of 10 to 100 erg / cm^2 [19]. In the paper [20] we have derived the explicit relation between the phase boundary surface tension and the term containing the Laplace operator of the equation for the order parameter. In our approach, we, therefore, account for the surface tension explicitly. The latter explains the difference between our results and those obtained in Refs. [17,18] and other papers [21].

In the presence of the surface tension, the cusp becomes energetically expensive since it has the infinitely small curvature radius. The surface tension, therefore, transforms a cusp into a smooth boundary portion, with a finite curvature radius, thus providing a setback and, therefore, a contact length [Fig. 10(ii)]. At $v = 0$, Eq. (6) predicts the dimensionless curvature radius in the form

$$\rho = \frac{1}{2^{1/3} v_G}. \tag{17}$$

In our simulations, it corresponds to the values summarized in Table I, the curvature radius given in the dimensionless units.

One finds the physical curvature radius at zero velocity R_0 in a standard way by multiplying these values by λ_0:

$$R_0 = \lambda_0 \rho. \tag{18}$$

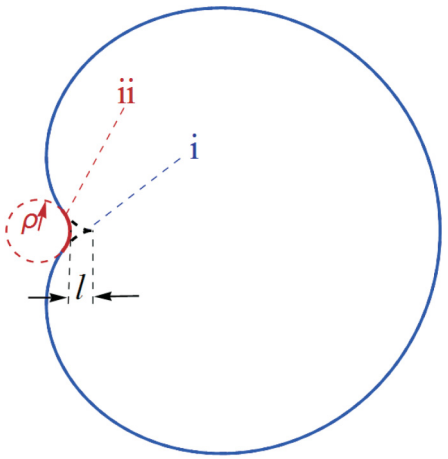

FIG. 10. Schematic view of the zone boundary. The blue part of the boundary coincides with the cardioid. (i) Indicates its cusp part. The solid red one (ii) is a smooth rear part of the boundary. The dashed red line shows a circle with the curvature radius ρ (6) inscribed into the cardioid. The contact length l between the crack tip and the invagination bottom is shown.

For example, in the case of $BaTiO_3$ and $PbTiO_3$ using λ_0 obtained above, one finds the curvature radius varying from $R_0 \approx 164$ nm at $a = 0.2$ down to about 29 nm at $a = 0.24$.

In Sec. IV of [1], we have observed that the simulation predicts a finite setback of the rear point of the zone (Fig. 10). In other words, the zone forms a smooth invagination, rather than a cusp. The smooth invagination exhibits a setback. That is, the zone boundary is displaced from the crack tip (0,0) to the point $(-l, 0)$ (Fig. 10). The contact length $l > 0$, thus, yields the quantitative measure of the setback.

In this paper, we demonstrated that the dimension of the contact length l of the motionless crack-zone complex varies between about 20 and 150 dimensionless units [Fig. 6(b)]. The latter by one to two orders of magnitude exceeds the thickness of the zone interface, which is about a few dimensionless units as we reported in [1]. For material parameters of $BaTiO_3$ and $PbTiO_3$ given above, the estimate for the contact lengths l at $v = 0$ yields the values varying from 200 nm to 1.5 μm.

One concludes that whatever the surface tension could be, it gives rise to a contact length l. It is along this distance that the zone is in the direct contact with the crack surface even when the crack is motionless. This contact length could be significant.

E. Wake observations

The physical time t is connected with the dimensionless one τ by the relation (10). Taking the typical size of the process zone observed in ferroelectrics $\Re \sim 1$ to 10 μm

TABLE I. The curvature radius of the invagination bottom at $v = 0$.

a	0.20	0.22	0.23	0.24
ρ	16.41	5.63	3.99	2.89

[11,22,23] and Gordon's velocity $V_G \sim 10^{-3}$ cm / s given above one finds for these materials the time of the wake decay $t_d \sim \Re/V_G \sim 0.1$ to 1 s. Such a small lifetime of the wake implies that it is only observable *in situ*, while the "post-mortem" wake detection in these materials is impossible. In general, the triangular wake is challenging to detect because it is only present in dynamics for a crack propagating with velocity $V > V_G$. So far, the lack of a theoretical prediction hindered the recognition of the metastable wake in experiments. Nevertheless, some observations indicating the metastable wake have been reported.

Isotov obtained an electron microscopic image of a crack Fe-Ni-Ti-Al alloy foil in the course of an unexpected formation and propagation of a crack caused by conditions of the sample fixation. This image unambiguously showed the triangular wake. With the kind permission of Isotov one of us has published this image in Fig. 1 in [24]. By the direct measurement of the zone height and the wake semivertex angle, one can find that in this case $V \approx 2.85V_G$.

Gollerthan and coauthors [25] observed that ≈ 2 mm sized zone of the martensite B19′ phase embedded in the bulk B2 austenite phase in NiTi. This zone forms at the tip of the crack upon loading and vanishes upon unloading [25]. During its propagation, the zone behind the crack was reported to vanish immediately [26]. On the one hand, one can interpret this observation as the case of a concave zone. On the other hand, in the case of a convex zone ($V > V_G$) if the value of V is high enough the wake is difficult to observe. Indeed, the values of V_G in NiTi as high as 370 m / s have been reported [27]. The thermographic image of a propagating crack [26] revealed two ≈ 1 mm long regions (petals) with the shapes of droplets at both faces of the crack behind the propagating B19′ process zone. Here, the material was considerably colder than that around the petals (see Figs. 3 and 4 in [26]). This temperature variation is due to the latent heat absorption during the backward endothermal B19′ → B2 transition at the rear boundary of the moving zone. The dropletlike shapes of the cold spots closely resemble the form of the triangular wake described here, which is suggestive that the wake indeed emerged behind the zone but rapidly vanished upon its propagation.

In Ref. [28], a mechanoluminescence effect has been used to study the stress-induced transformation in yttria-zirconia ceramics *in situ* during the crack propagation. Strong luminescence irradiation indicated the region of the solid transformed into the monoclinic phase. The latter represented a 590 μm spot at the tip of the motionless crack. Upon the crack propagation with the velocity of 20 to 140 m/s, it stretched out up to about 6 mm in length. In light of our results, one interprets the observed evolution as a zone at the motionless crack tip stretching out into the zone and wake complex and then following the crack tip motion. An immediate reverse transformation of martensite into austenite behind a slowly propagating crack-process zone complex has been observed in NiAl [29], suggesting a zone with no wake.

IV. SUMMARY

In summary, we studied a process zone at the tip of a propagating crack. In the previous paper [1] by simulation, we demonstrated that with increasing the crack speed, the zone shape changes from the concave to the convex one. The former shape exhibits an invagination in the rear part of the zone, while the latter shape resembles a droplet and exhibits a triangular metastable wake. The zone-wake system propagates with the speed of the crack.

In this paper, we communicated geometric parameters the zone and the wake obtained from the numerical experiment. We demonstrate that these parameters rapidly grow with approaching the binodal on the phase diagram but dramatically decrease with the increasing the crack velocity. Simultaneously, the wake becomes longer and sharper. The zone vanishes at a critical value of the crack speed.

ACKNOWLEDGMENT

A.L.K.'s work was supported by the RNF under Project No. 19-19-00552.

[1] A. Boulbitch and A. L. Korzhenevskii, Phys. Rev. E **101**, 033003 (2020).
[2] L. D. Landau and E. M. Lifshitz, *Statistical Physics*, 3rd ed. (Pergamon, Oxford, 1985).
[3] J. C. Toledano and P. Toledano, *The Landau Theory of Phase Transitions* (World Scientific, Singapore, 1987).
[4] A. Gordon, Phys. Lett. A **99**, 329 (1983).
[5] A. Gordon, I. D. Vagner, and P. Wyder, Phys. Rev. B **41**, 658 (1990).
[6] L. Bakaleynikov, J. Felsteiner, and A. Gordon, Phys. B (Amsterdam) **369**, 104 (2005).
[7] A. Boulbitch and A. L. Korzhenevskii, Eur. J. Phys. B **89**, 261 (2016).
[8] M. L. Lines and A. M. Glass, *Principles and Applications of Ferroelectrics and Related Materials* (Oxford University Press, Oxford, 2001).
[9] R. C. Pohanka, S. W. Freiman, and B. A. Bender, J. Am. Ceram. Soc. **61**, 72 (1978).
[10] R. C. Pohanka, S. W. Freiman, and R. W. Rice, Ferroelectrics **28**, 337 (1980).
[11] F. Meschke, O. Raddatz, A. Kolleck and G. A. Schneider, J. Am. Ceram. Soc. **83**, 353 (2000).
[12] L. Q. Chen, in *Physics of Ferroelectrics: A Modern Perspective*, edited by K. M. Rabe, C. H. Ahn and J. M. Triscone (Springer, Berlin, 2007), Vol. 105, pp. 363–371.
[13] A. Gordon, Phys. B (Amsterdam) **138**, 239 (1986).
[14] J. C. Burfoot and T. J. Parker, Brit. J. Appl. Phys. **17**, 213 (1966).
[15] S. M. Yufatova, Y. G. Sindeyev, V. G. Gavrilyatchenko, and E. G. Fesenko, Ferroelectrics **26**, 809 (1980).
[16] R. M. McMeeking and A. G. Evans, J. Am. Ceram. Soc. **65**, 242 (1982).
[17] B. Budiansky, J. W. Hutchinson, and J. C. Lambropoulos, Int. J. Solids Struct. **19**, 337 (1983).
[18] C. Lexcellent and F. Thiebaud, Scripta Mater. **59**, 321 (2008); A. Falvo, F. Furgiuele, A. Leonardi, and C. Maletta,

J. Mater. Eng. Perform. **18**, 679 (2009); V. Taillebot, C. Lexcellent, P. Malecot, and R. Laydi, Eur. Symp. Martensitic Transform. **2009**, 06034 (2009).

[19] A. G. Khachaturian, *Theory of Structural Transformations in Solids* (Wiley, New York, 1983); T. Kruml, B. Viguier, J. Bonneville, and J. L. Martin, Mater. Sci. Eng. **234**, 755 (1997); B. Meyer and D. Vanderbilt, Phys. Rev. B **65**, 104111 (2002); V. Kokotin and U. Hecht, Computat. Mater. Sci. **86**, 30 (2014); T.-K. Tsao and A.-C. Yeh, Mater. Trans. **56**, 1905 (2015); Y. Fan and M. M. Malhlouf, J. Metals Comp. **725**, 171 (2017); W. Li, J. Ma, H. Kou, J. Shao, X. Zhang, Y. Deng, Y. Tao, and D. Fang, Int. J. Plasticity **116**, 143 (2019).

[20] A. Boulbitch and A. L. Korzhenevskii, Phys. Rev. B **96**, 054106 (2017).

[21] P. M. Kelly and L. R. F. Rose, Prog. Mater. Sci. **47**, 463 (2002).

[22] S. O. Kramarov, N. Y. Egorov, and L. M. Katsnel'son, Fiz. Tverd. Tela **28**, 2858 (1986) [Sov. Phys.–Solid State **28**, 1602 (1986)].

[23] X. Tan, S. E. Young, Y. H. Seo, J. Y. Zhang, W. Hong, and K. G. Webber, Acta Mater. **62**, 114 (2014).

[24] A. A. Bulbich, J. Mater. Sci. **27**, 1070 (1992).

[25] S. Gollerthan, M. L. Young, K. Neuking, U. Ramamurty, and G. Eggeler, Acta Mater. **57**, 5892 (2009).

[26] S. Gollerthan, M. L. Young, A. Baruj, J. Frenzel, W. Schmahl, and G. Eggeler, Acta Mater. **57**, 1015 (2009).

[27] J. Niemczura and K. Ravi-Chandar, J. Mech. Phys. Solids **54**, 2136 (2006).

[28] J. S. Kim, H. J. Koh, W. D. Lee, N. Shin, J. G. Kim, K.-H. Lee, and K.-S. Sohn, Met. Mater. Int. **14**, 165 (2008).

[29] U. D. Hangen and G. Sauthoff, Intermetallics **7**, 501 (1999).